Chapter 3

Ferromagnetism in C-doped ZnO Thin Films*

In this chapter we report on the observation of room temperature ferromagnetism in carbon-doped ZnO thin films prepared by electron beam evaporation. Magnetization, Hall effect, X-ray photoemission spectroscopy and X-ray diffraction studies were conducted to investigate the source and nature of ferromagnetism. The samples were found to show *n*-type conduction with a carrier concentration which increases with C doping. The photoemission data give evidence for C substitution at the zinc site and are consistent with the formation of C-O bonds. The ferromagnetism is suggested to originate from Zn vacancies that are stabilized when C is incorporated at zinc sites.

---

*The results presented in this chapter were published in:
S. Akbar, S. K. Hasanain, Manzar Abbas, S. Ozcan, B. Ali, S. Ismat Shah, "Defect induced ferromagnetism in carbon-doped ZnO thin films", Solid State Communications, 151(1), 17–20 (2011).

3.1 Introduction

Ferromagnetism has been reported in nanoparticles or thin films of nonmagnetic materials without any dopant[1-3]. The question of why ferromagnetism occurs in doped semiconductors is complicated by the fact that most X-ray magnetic circular dichroism (XMCD) measurements do not detect any ferromagnetic moment on the transition metal dopants[4], and instead clustering of the magnetic dopants has been suggested[5]. However, several recent studies of ferromagnetism associated with nonmagnetic dopants in semiconductors do not support clustering of magnetic ions[6, 7]. It is also known that intrinsic defects of the host play a critical role in stabilizing ferromagnetism in such systems. This stabilization may occur either by creating defects at the surface or at grain boundaries (associated with an enhanced density of states localized there) or, as in the case of Zn vacancies[2], by altering the charge distribution in the vicinity of the vacancy and creating a moment on the O ion. Pan *et al*. observed room temperature ferromagnetism in C-doped ZnO and their findings were confirmed by first-principle calculations[7]. They assumed that C substituted for the O atoms and a hole mediated mechanism was proposed for ferromagnetism in C-doped ZnO. On the other hand, Ye *et al*.[8] reported that hole generation in C-doped ZnO powders actually resulted both in the decrease of the electron density and of the magnetic moment, and proposed an electron mediated mechanism for the same system. To our knowledge, X-ray photoelectron spectroscopy (XPS) measurements on these systems did not establish unambiguously whether C is substituting for O (C_O) or Zn (C_{Zn}) [9, 10]. Hsu *et al*.[11] suggested that even if the C dopants are not at C_O sites, C is still a novel dopant which drives ferromagnetism (FM) in ZnO by controlling the defects created by loss of carbon during suitable post-annealing of C:ZnO films. Mishra *et al*.[12] reported an enhancement of FM in carbon-doped ZnO nanostructures as compared to pure ZnO. They observed that FM in carbon-doped ZnO arises from the creation of defects or the development of oxy-carbon clusters. From formation energy calculations they also confirmed from formation energy calculations that carbon substitution at oxygen site in ZnO lattice is thermodynamically rather unfavourable for the common environmental conditions in the experiment. A DFT study by Sakong *et al*.[13] showed that in carbon-doped ZnO, carbon substituting at the zinc site (C_{Zn}) represents the defect with the highest absolute stability, followed by the C_{Zn}–C_i complex. Interstitial C in *n*-type ZnO prefers to form interstitial pairs or C_{Zn}–C_i complexes, which lowers the defect formation energy. These

authors identified in both *p*-type and *n*-type ZnO certain charge states of C_{Zn}–C_i complexes, which possess a spin magnetic moment and might explain why both *p*-type and *n*-type magnetism has been reported for C-doped ZnO. Amiri *et al*.[14] showed that both Zn vacancies and the presence of C defects (substitutional, interstitial or combination of both) induce the ferromagnetism in C-doped ZnO and the mechanism of ferromagnetic coupling is the *p*–*p* interaction between C atoms and/or C and O atoms. The very limited experimental verification of ferromagnetism in C-doped ZnO and the obvious discrepancies between the results[7, 8] suggest that more work needs to be done. In particular, it also needs to be determined whether the observed ferromagnetism is connected to C substituting for O or Zn or whether some defect structures with magnetic moment are formed. To elucidate these issues, we investigated the magnetic and electronic properties of C-doped ZnO thin films deposited by electron beam evaporation on different glass substrates.

3.2 Experimental details

Pristine ZnO and C-doped ZnO thin films were deposited on soda lime and Corning glass(0120) by electron beam evaporation as explained in chapter 2. The base pressure attained in the chamber was about 2.3×10^{-6} mbar and the evaporation source-to-substrate distance 12 cm. Three different targets were prepared by grinding ZnO (99.9 %) and graphite (99.9 %) powders together. The thickness of the films and the deposition rate were controlled with the help of an *in-situ* quartz crystal thickness monitor. The nominal thickness of the films investigated here was ~300 nm and the deposition rate 5 Å/sec. All the films were deposited at room temperature and subsequently annealed at 500 °C in air for 1 h. Before annealing, the films were amorphous as verified by X-ray diffraction (XRD) (the technique is explained in chapter 2) and black in colour. After annealing, these films became crystalline and almost transparent with a slight milky shade. The carbon concentration was estimated by chromatography (CHNS scan). The nominally 1 at.% C sample was found to contain 0.25 at.% C while the nominally 3 at.% sample contained 1.9 at.% carbon. The C-doped ZnO films with 0.25 and 1.9 at.% C will be referred to as samples #1 and #2 respectively. Another thin film of C-doped ZnO was also grown by a different technique. Initially, we grew a ~300 nm undoped ZnO film on the Corning (0120) glass substrate by electron beam evaporation. Next, we deposited a thin layer of carbon on it, using a pulse arc discharge technique[15]. Subsequently this type of film was annealed at 550 °C for 1 h in air. We

shall refer to this sample as sample #3 in the following. Electrical resistivity, carrier concentration and mobility were measured by the Hall effect setup described in Chapter 2. Aluminium ohmic contacts to the ZnO thin films were prepared by thermal evaporation. The crystal structures of the films and bulk samples were characterized by X-ray diffraction (XRD) in a 2θ range 20°–70° as described in Chapter 2. X-ray photoelectron spectroscopy (XPS) measurements were performed as described in Chapter 2. The binding energy was referenced to the C 1*s* peak at the binding energy of 285.0 eV unless specified otherwise. Magnetic measurements performed by Physical Property Measurement System (PPMS, Quantum design) as detailed in Chapter 2.

3.3 Result and discussions

3.3.1 X-ray diffraction analysis of thin films

XRD results for the pure ZnO film, as well as for the C-doped samples #1, #2, and #3 are shown in Figure 3.1. (a-c) The observed peaks correspond to the Wurtzite structure, confirming the development of the desired phase. No unidentified peaks were observed. The intensity of the (002) peak shows that all the films preferentially exhibited the (002) orientation, which has been reported in the literature[16]. No other C phases were observed by XRD. Comparison of the relative intensities of the three main XRD peaks reveals that the intensity of the (002) peak is the highest in the pure ZnO thin film and decreases with C content. Figure 3.1 (b) shows a clear broadening of the XRD peaks with increasing C content, evidenced also by the plot of the increase in full width at half maximum (FWHM) values with carbon content presented in Figure 3.1 (c). This broadening of the peaks may stem from the distortion of the host lattice due to the strain induced by C occupying zinc sites or interstitial sites. This indicates that the preferred growth of the films along the (002) direction becomes less dominant upon C incorporation. The lattice constants *a* and *c*, calculated from the (100) and (002) planes respectively, are shown in Figure 3.2 (a, b) for the different films.

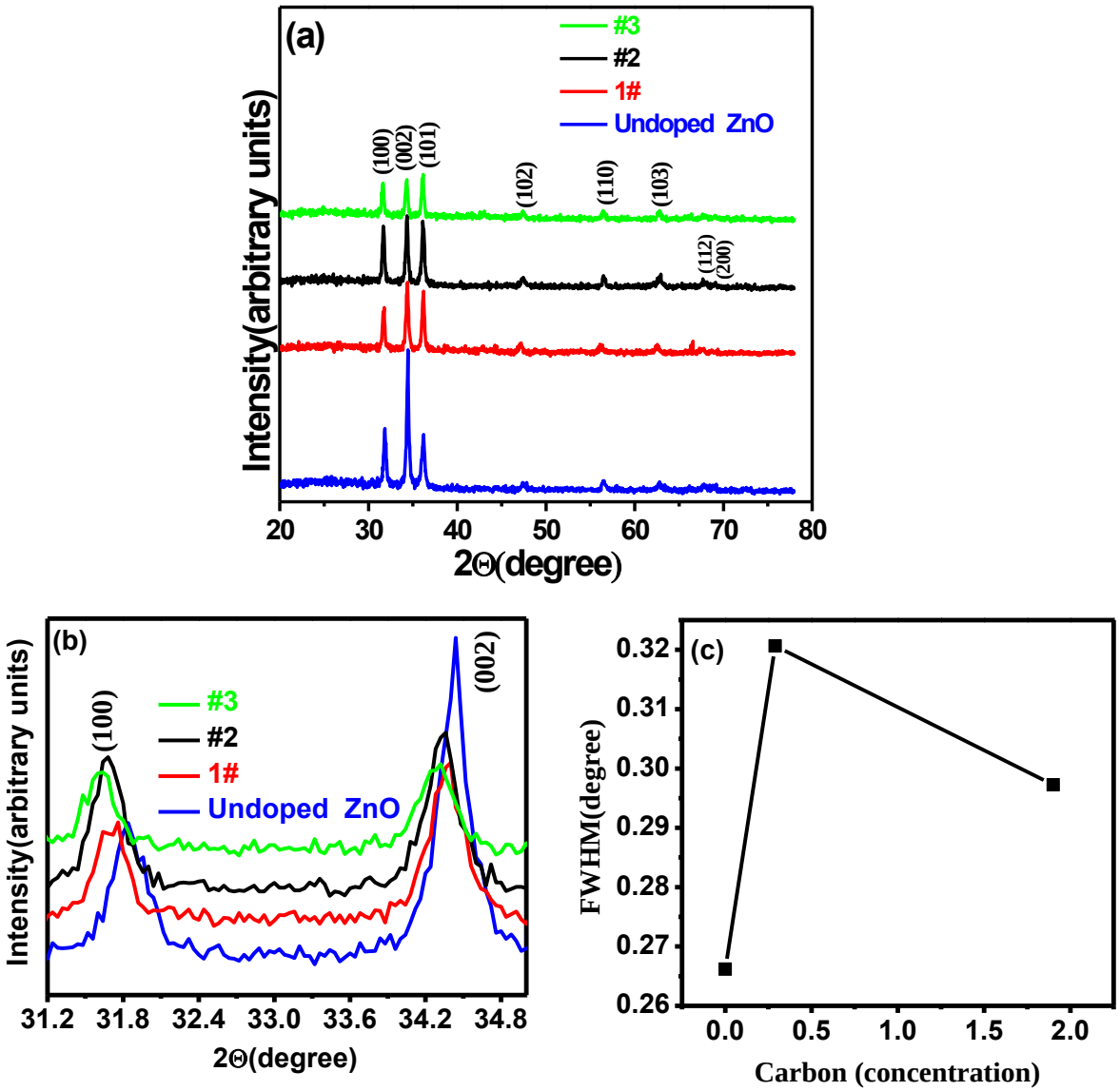

Figure 3.1 (a) X-ray diffraction patterns of undoped and carbon-doped 300 nm thick ZnO films annealed at 500 °C. (b) The enlarged XRD patterns of undoped ZnO, #1, #2 and #3 C-doped ZnO samples. (c) Variation of full width half maximum (FWHM) values of the (002) peak with Carbon concentration.

The lattice constants show a marked decrease for the #1 sample C-doped films (a = 3.246 Å, c = 5.204 Å) as compared to the undoped films (a = 3.250 Å, c = 5.209 Å). However, sample #2 showed a significant increase in both the lattice constants (a = 3.251 Å, c = 5.215 Å) as compared to the sample #1. An increase in 2θ values as compared to XRD data of pure ZnO has been reported earlier for C-doped ZnO nanocrystals[17]. We note that the radius of the Zn^{2+} ion is 0.74 Å,[18] while that of O^{2-} is 1.4 Å [19].

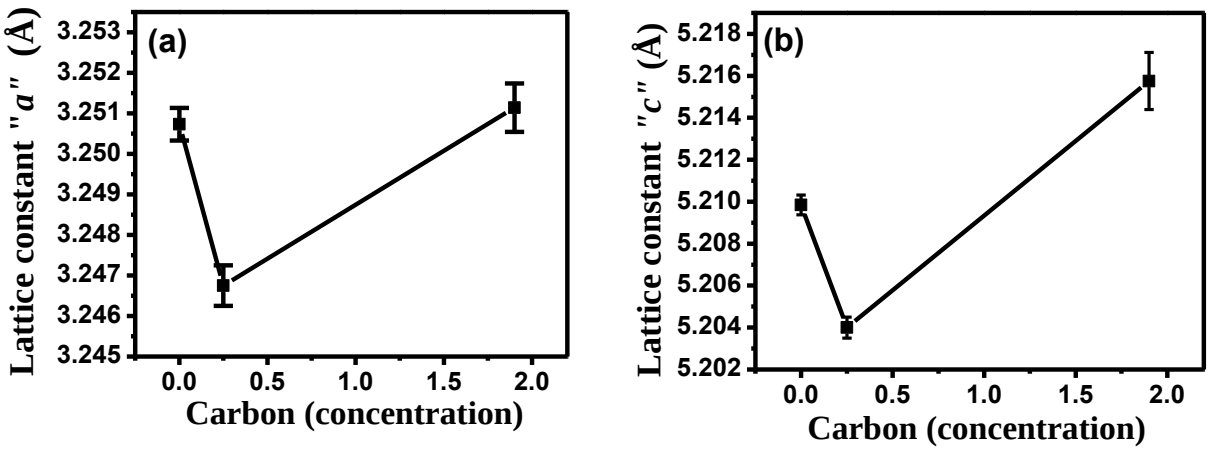

Figure 3.2 Variation of lattice parameters (a) "a" and (b) "c" in carbon-doped ~300 nm thick ZnO films with different carbon concentration.

On the other hand the possible ionic sizes of C are 2.60 Å for the −4 state[20] and 0.30 Å for the +4 state[21]; the covalent radius[22] is about 0.77 Å. The decrease of the ZnO lattice constant for the #1 sample composition suggests that C is incorporated at the Zn sites. Incorporation at the O sites as an anion would lead to larger lattice constants[8, 14]. The radius of covalent carbon is smaller than the radius of O^{2-}; a reduction of lattice constant with carbon doping could therefore also be expected when carbon ions are incorporated into the O site of the ZnO lattice [23]. However C substitution for Zn was confirmed by XPS results (*vide infra*) but there is no evidence for carbon substitution at the oxygen site (C_O). The lattice constant *c* of the #2 sample is less than that of the undoped film but higher than that of the #1 sample. It is possible that in this case the C atoms may be at least partially incorporated into interstitial sites, leading to a larger lattice constant.

3.3.2 Electrical measurements

Hall effect measurements at room temperature were performed on both pure ZnO and on the #2 sample in the configuration described in chapter 2. Our measurements showed *n*-type conductivity for both cases. For the C-doped sample an increased carrier concentration almost a factor of three was observed, from $n = 5.7 \times 10^{16}/cm^3$ for the pure ZnO to $n = 1.7 \times 10^{17}/cm^3$ for the #2 sample. The low resistivity values (58.0±0.2 and 23.0±0.2 Ohm•cm for the pure and C-doped films, respectively) confirm the good quality of inter-grain contacts in these films. *n*-type

conductivity in ZnO has been attributed to the presence of intrinsic defects such as oxygen vacancies (V_O), and zinc interstitials (Zn_i)[24]. On the other hand O substituted with C are expected to act as acceptor impurity in ZnO. Both *n*-type[7, 8] and *p*-type conduction[10] have been reported in C-doped ZnO. Pan *et al*.[7] have reported an increase in the electron concentration with C doping but argued that the holes expected to be formed by C doping were masked by the intrinsic electron defects. Ye *et al*.[8] observed a decrease in the electron concentration and a degradation of ferromagnetism due to annealing in a nitrogen (hole generating) environment. Our Hall effect results are consistent with those of Ref. 8, in the sense that we observe *n*-type conductivity and find that the addition of C enhances the electron concentration.

3.3.3 X-ray photoelectron spectroscopy analysis

XPS allows to determine the ionic state of the constituents or the dopants and to infer the possible bonding of the dopants with the host. XPS data for the Zn 2*p*, O 1*s* and C 1*s* binding energy regions are shown in Figure 3.3 (a, b, c) for the samples #1, #2 and #3. The Zn 2*p* region in Figure 3.3(a) shows two peaks, which correspond to the reported binding energies (BE) for Zn $2p_{3/2}$ and Zn $2p_{1/2}$ states[25].

The BEs of Zn $3p_{3/2}$ line for film #1 and film #3 is (1021.2 eV) while that of #2 is shifted to a higher value (1021.9 eV). It is significant to note that the former two films display stronger ferromagnetic properties than the latter, as will be discussed below. The C 1*s* spectrum, shown in Figure 3.3(c), can be de-convoluted into two peaks labeled as C1 and C2. The major peak at the lower binding energy C1 was attributed to the ‘‘free carbon’’ (graphite or carbon contamination) at 285 eV, while the smaller peak at a higher binding energy C2 (286.5 eV) is due to C in the ZnO matrix. When C substitutes O, the C 1*s* binding energy shifts to a slightly lower value[7]. However, in the case of carbon atoms substituted at the zinc site, there is the possibility of the O-C–O bond (286.1 eV) with binding energies higher than for free carbon[9]. This situation can lead to the development of two main C-related defects, *i.e.* carbon substituting for Zn (C_{Zn}) or carbon substituting for Zn and combining with two interstitial oxygen atoms to form a carbon-interstitial oxygen defects ($C_{Zn} + 2O_i$).

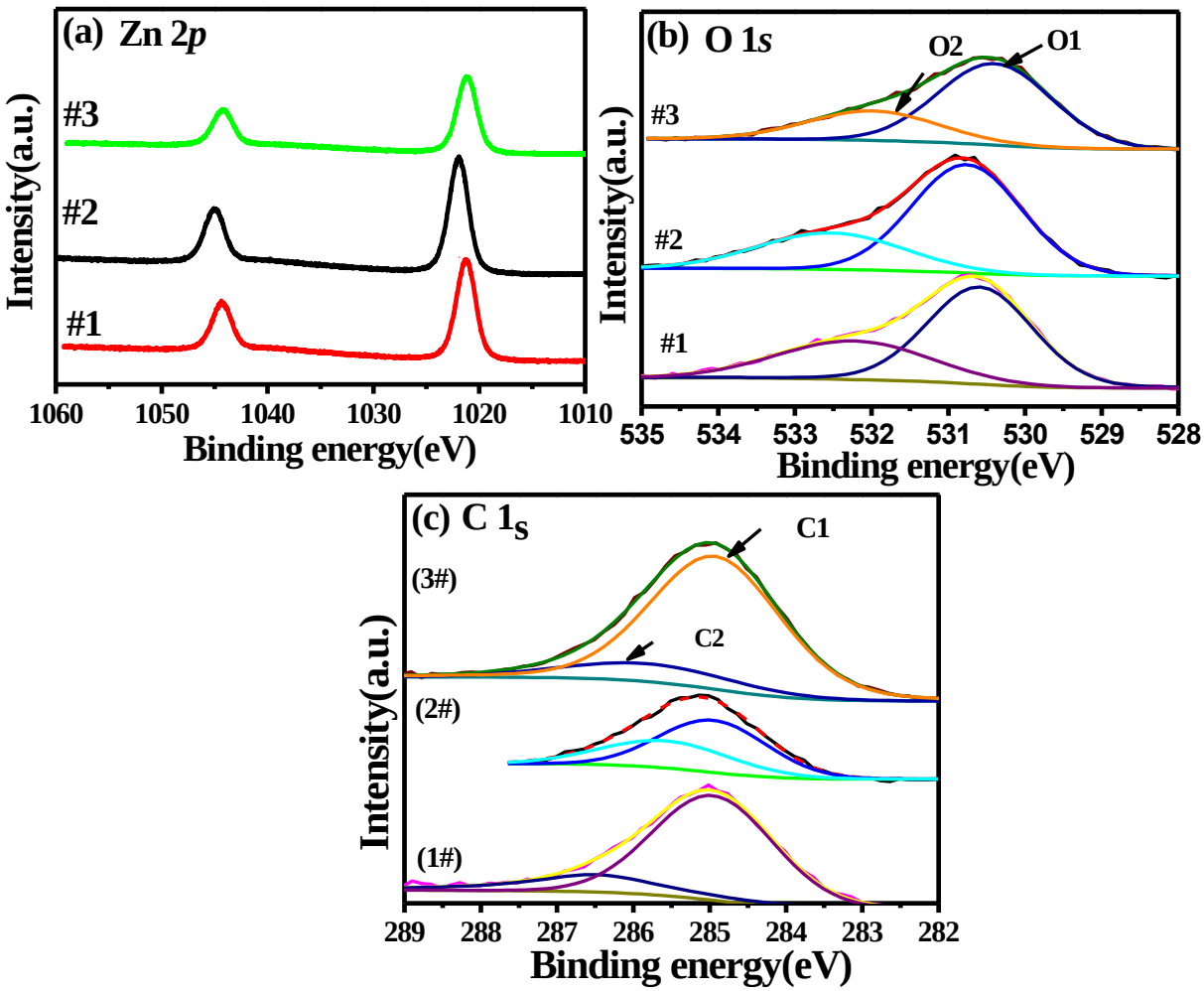

Figure 3.3 XPS spectra of (a) Zn 2*p*, (b) O 1*s* and (c) C 1*s* core level regions of #1, #2 and (#3) samples. Data (black line) and fits (coloured line) are shown (for details see text).

A major difference between these two types of C_{Zn} defects is that the carbon substituting for Zn is an *n*-type defect, while the C–O complex is of *p*-type[9]. It has been estimated[9] that the formation energies of other defects such as C_O (C substituted for O) are prohibitively higher and become more so at lower oxygen partial pressures. The absence of any lower binding energy peak in our XPS spectrum suggests that C is not substituting for oxygen. Our results are more consistent with the formation of C–O bonds and with the presence of C primarily in the +4 state as also supported by XRD results. The fundamental difference between C substituting for O and C substituting for Zn is that the former has been shown by density functional theory calculations[7] to be related to the stabilization of hole mediated ferromagnetism. The binding energy position of the C 1*s* peak correlates with the type of ferromagnetism: when it is lower than 250 eV, *p*-type ferromagnetism was observed[7], while in the opposite case[8], namely for binding energies higher

than that for free carbon, *n*-type ferromagnetism was observed. WC is the presence of C in a higher than divalent state, *e.g.* C^{+4} as explored by our XPS measurements.

Continuing with the XPS analysis, we note that the O 1*s* spectra shown in Figure 3.3 (b) can be deconvoluted into two peaks at BE of 530.54 and 532.54 eV, respectively. These spectra are typical of ZnO, where the low binding energy component is attributed to O^{2-} ions of the Wurtzite structure of the hexagonal Zn^{2+} ion array, surrounded by Zn atoms[26]. The higher binding energy peak has been attributed to different reasons, *e.g.* oxygen vacancies, hydroxyl groups or absorbed oxygen[9]; it has been found to grow with low oxygen partial pressure and hence often been assigned to the presence of oxygen vacancies[27]. In our case where the films were annealed in ambient air, oxygen vacancies cannot be ruled out but the number of oxygen vacancies is expected to be low compared to that found for films annealed in a reducing atmosphere. This O 1*s* higher binding energy peak can also be attributed to the C–O bond in a defect complex that comprises of a carbon atom substituted for zinc (C_{Zn}) and two interstitial oxygen ions[9].

Thus our XPS results suggest that the C atoms are substituting for the zinc atoms and also indicate the possibility of defect complexes that involve C–O bonds[17].

3.3.4 Magnetization measurements

The magnetic studies were performed on all four types of samples, the pure ZnO films, #1, #2 and #3 sample. Each of these samples showed room temperature ferromagnetism. To eliminate any possible contribution to the observed ferromagnetism from the substrate, each substrate alone was studied separately. The room temperature (positive) moment of the glass substrate (not shown here) was determined to be ~1×10^{-5} emu at 1 kOe applied field; the moment becomes diamagnetic at higher applied fields. On the other hand the undoped ZnO films on the glass substrate showed a diamagnetic moment of ~ -9.8×10^{-7} emu at the same field. The Corning glass substrate had a diamagnetic moment of -1.2×10^{-6} emu at 1 kOe as shown in Figure 3.4 (a). The hysteresis loops for samples #1, #2 and #3 taken at room temperature are shown in Figure 3.4 (b) without subtraction of the substrate contribution.

From the data it is clear that at least for the #1 sample and the C-coating coated film (#3 sample) the ferromagnetic moment is well in excess of any contributions from the substrate. At 1 kOe, #1sample has a moment which is 50 times larger than that of the substrate itself, while

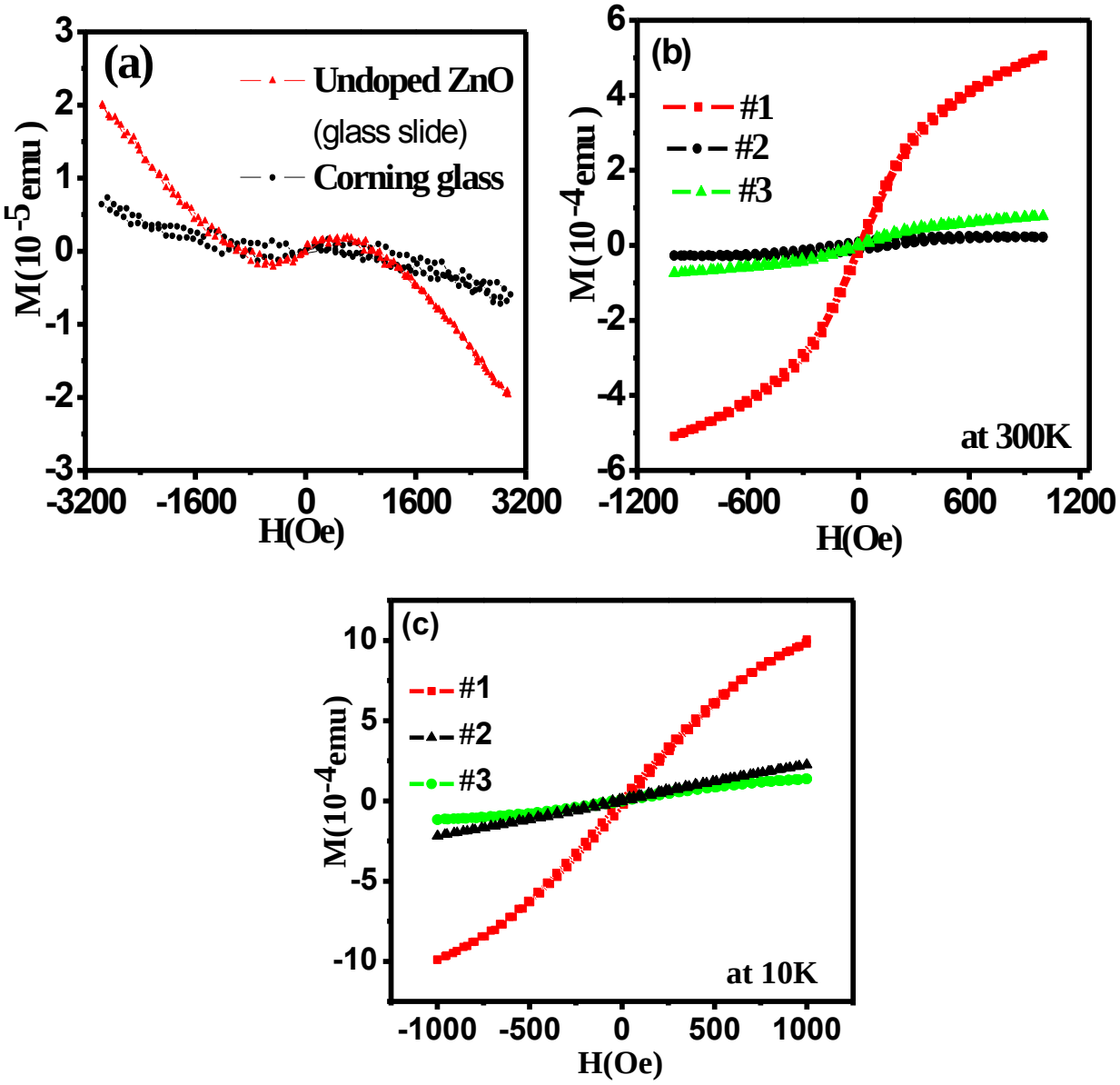

Figure 3.4 Hysteresis loops for (a) Undoped ZnO (on glass slide) and Corning glass at room temperature and #1, #2 and #3 samples at (b) 300 K and (c) 10 K

#3 sample has a ferromagnetic signal of $+7.8 \times 10^{-5}$ emu (5.7 emu/cm^3) where the substrate itself has a diamagnetic signal of the order of -1×10^{-6} emu. The ferromagnetic moment of the #2 sample was about twice as much as the positive moment from the substrate; hence the contribution from C-doped ZnO may seem questionable. However considering that the ZnO matrix plus glass substrate combined have a diamagnetic contribution of ~ -9.8×10^{-7} emu, the observed ferromagnetic moment of ~ $+2 \times 10^{-5}$ emu (1.8 emu/cm^3) in this sample also appears to

be quite significant. Thus for all these films room temperature ferromagnetism is clearly observable as a consequence of C incorporation into the ZnO matrix. The strongest moment is seen in the case of #1 sample. Pan *et al.*[7] have shown that the saturation magnetization increases strongly between 0 and 1 at.% C doping, followed by a slow increase up to about 5 at.% but decreases for higher C content. According to Zhou *et al.*[20] the highest saturation magnetization is achieved at 2 at.% C and reduced values are observed for higher C doping. Earlier reports, both theoretical[14, 28] and experimental[7, 20], have shown a non-monotonic variation of the magnetic moment with increasing C content of ZnO thin films. This behaviour has been interpreted as a sign for the carbon atoms distributing non-uniformly at higher concentrations. Thus we conclude that the decrease in the moment for our #2 composition is most likely due to the increased presence of C atoms in interstitial positions. Such interstitial C suppresses the magnetic moment since the single C_i defect is non-magnetic[13].

The temperature dependence of the magnetization was analysed for the C-coated ZnO film on the Corning glass substrate. The temperature dependence of the other films was not analysed due to the substantial temperature dependence of the magnetization of the glass substrate. The Corning glass substrate had a small diamagnetic contribution all the way to 50 K as shown in Figure 3.5 (a). Below 50 K the moment of the substrate begins to show a significant upturn. Hence the M(T) data selected for fitting were confined to the temperature region T > 90 K. The data were fitted with the Bloch law $M(T) = M(0)\ (1-(T/Tc)^n)$ expected for a spin wave contribution. The result of the fit is shown in Figure 3.5 (b). The parameters obtained from the fit were n=2.02±0.07 and T_c=501.0±8.6 K. The larger value of the Bloch exponent, *i.e.* 2 as opposed to the value of 1.5 expected for spin waves in a 3 dimensional system, has been observed often in systems with finite size effects such as nanoparticles and nanometer thick films and attributed to the quantization of spin wave and the occurrence of a size-dependent gap in the spin wave spectrum[29, 30]. The value of T_c obtained from the fit is consistent with the observation of ferromagnetism at room temperature and its high value of 501 K indicates strong ferromagnetic coupling. Hence the analysis of spin wave behaviour in the C doped films appears to suggest 3-d ferromagnetism with a more rapid decrease of moment with temperature than in a bulk ferromagnet, possibly due to the finite size of the ferromagnetic regions.

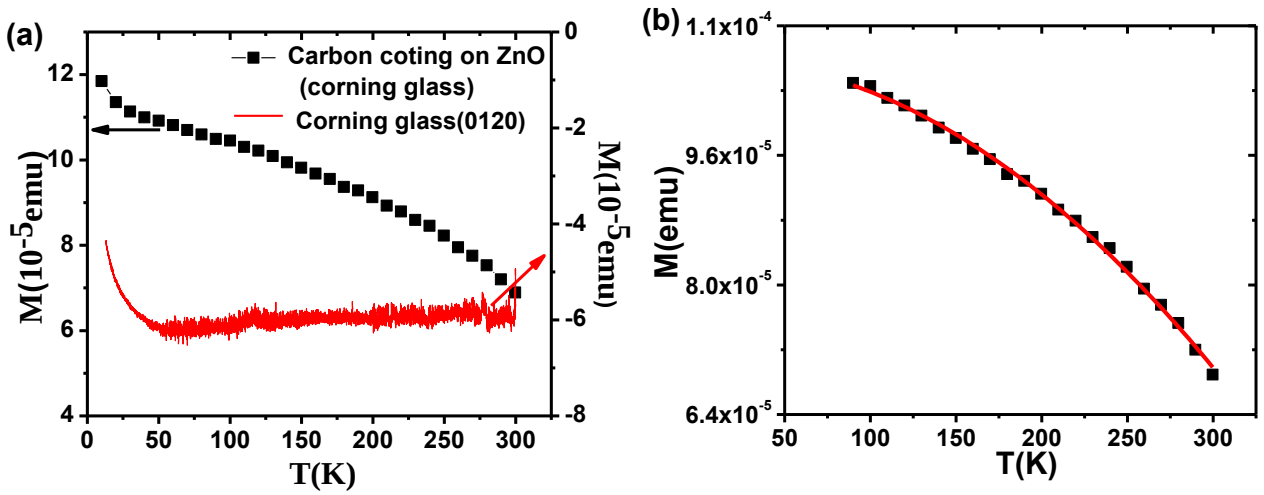

Figure 3.5 (a) Temperature dependence of magnetization of a carbon-coated ZnO film and of the Corning glass substrate. The applied field was 1 T. (b) Bloch law fit to the M-T data of (a), 90 K<T<300 K.

3.4 Conclusions

Our data clearly shows the presence of RT ferromagnetism in C-doped ZnO thin films that exhibit *n*-type conductivity. Several scenarios may be invoked to explain the mechanism of this FM and the other trends in the XPS and XRD measurements. At this stage it is however possible to draw some broad conclusions from the available data. We note that many of the recently studied models are based on the substitution of C for oxygen and the consequent hybridization between Zn and C orbitals. The localized holes produced by the Zn-C bond generate the moment in this model. However our XPS data do not give any clear indication for C_o defects (no C 1*s* component at lower binding energy than that of free carbon), which form the basis of this model. The XRD data indicating the reduction of the lattice constant are consistent with both C_{Zn} and C_o. The presence of oxygen vacancies is also inferred from the XPS. In searching for alternate explanations consistent with the data we note that according to the defect induced ferromagnetism model, Zn vacancies in ZnO can lead to a spin polarized solution with magnetic moment of 2 μ_B/Zn vacancy. Furthermore co-doping of nonmagnetic ions, *e.g.* Li[31], support FM in ZnO by reducing the formation energy of the zinc vacancy. In the same spirit we can consider the observed RT ferromagnetism in C-doped ZnO as being caused by the stabilization of the Zn vacancy by lowering its formation energy at Zn sites nearby the C atom[12, 32]. While a zinc

vacancy is generally a high energy defect, its formation is relatively easier on surfaces or in the presence of a suitable dopant[6]. A possible source for the stabilization of Zn vacancies by C is the presence of C in a higher than divalent state, *e.g.* C^{+4}. This possibility cannot be ruled out in the light of our XRD measurements, which show a decrease of the lattice constant with C incorporation. The presence of C in a higher valence state would generate an excess of electronic charge and the excess charge can be compensated by the generation of zinc vacancies.

We argue along the lines of references [2, 3] that Zn vacancies lead to unpaired O electrons in their immediate neighbourhood, which provide the moment, while the coupling between these unpaired O 2*p* electrons can then lead to the development of room temperature ferromagnetism. It therefore appears that room temperature ferromagnetism in *n*-type C-doped ZnO may occur, distinct from ferromagnetism in *p*-type C-doped ZnO, as an example of defect ferromagnetism generated by the stabilization of zinc vacancies.

The possibility of ferromagnetism in C-doped ZnO with carbon substitution at the oxygen sites (C_O) has been discussed by various authors[7, 8, 20, 23, 33-35]. Despite the fact that our XPS data do not show the expected Zn-C bond component at a lower binding energy, our XRD data are consistent with the expectations of this model. For example the substitution of O by C is expected to reduce the lattice constant due to the smaller size of the C ions compared to that of the O ions (the radii of O^{2-} and covalent carbon are 1.40 Å and 0.77 Å (respectively)[22]. Hence the reduction of lattice constant compared to ZnO is consistent with the expectation of C substituting at O sites in the ZnO lattice.[23] In fact, the increase in the lattice constant with higher C concentrations can only be explained if C is assumed to occupy interstitial sites for higher concentrations[8, 20, 33, 36]. Furthermore our XPS measurements show the presence of a (weaker) peak at higher binding energy assigned to the presence of zinc oxy-carbide complexes. However in the literature this peak has also been interpreted as indicating the existence of carbon substituting for oxygen and resulting formation of Zn–C bonds[33]. The bonding of C with Zn atoms leads to C 2*p*–Zn 3*d* hybridization and the resulting magnetic moment is due to the transfer of an electron from the *d* orbital of the Zn ion to the *p* orbital of the C ion. With the transfer of a *d* electron, the Zn *d* orbital changes from d^{10} (completely filled) to d^9 (incompletely filled) state. Finally FM can be induced by the polarization of itinerant electrons originating from O vacancies[8]. The presence of O vacancies is not only expected but strongly suggested by our XPS measurements. Mishra *et al.*[12] have discussed a different version of the defect-induced mechanism responsible for

ferromagnetism in C-doped ZnO. They have argued that the FM arises from the creation of defects or the development of oxy-carbon clusters.

Hence it appears that while the specific mechanism is uncertain on the basis of these measurements, it is definitely a case of defect induced ferromagnetism where the substitution of C within a defect complex whereby Zn-C bond may be formed, or C as a stabilizer of Zn vacancy, could be leading to the stabilization of FM in C-doped ZnO. Some of the measurements to be described in chapter 4 shed more light on the role of electrons or holes in the mechanism of ferromagnetism prevailing in C-doped ZnO thin films.

References

1. N. H. Hong, J. Sakai, W. Prellier, A. Hassini, A. Ruyter and F. Gervais, Physical Review B **70** (19), 195204 (2004).

2. Q. Wang, Q. Sun, G. Chen, Y. Kawazoe and P. Jena, Physical Review B **77** (20), 205411 (2008).

3. S. Kumar, Y. J. Kim, B. H. Koo, S. Gautam, K. H. Chae, R. Kumar and C. G. Lee, Materials Letters **63** (2), 194-196 (2009).

4. A. Ney, K. Ollefs, S. Ye, T. Kammermeier, V. Ney, T. C. Kaspar, S. A. Chambers, F. Wilhelm and A. Rogalev, Physical Review Letters **100** (15), 157201 (2008).

5. M. Opel, K. W. Nielsen, S. Bauer, S. T. B. Goennenwein, J. C. Cezar, D. Schmeisser, J. Simon, W. Mader and R. Gross, The European Physical Journal B **63** (4), 437-444 (2008).

6. J. B. Yi, C. C. Lim, G. Z. Xing, H. M. Fan, L. H. Van, S. L. Huang, K. S. Yang, X. L. Huang, X. B. Qin, B. Y. Wang, T. Wu, L. Wang, H. T. Zhang, X. Y. Gao, T. Liu, A. T. S. Wee, Y. P. Feng and J. Ding, Physical Review Letters **104** (13), 137201 (2010).

7. H. Pan, J. B. Yi, L. Shen, R. Q. Wu, J. H. Yang, J. Y. Lin, Y. P. Feng, J. Ding, L. H. Van and J. H. Yin, Physical Review Letters **99** (12), 127201 (2007).

8. X. J. Ye, H. A. Song, W. Zhong, M. H. Xu, X. S. Qi, C. Q. Jin, Z. X. Yang, C. T. Au and Y. W. Du, Journal of Physics D: Applied Physics **41** (15), 155005 (2008).

9. S. T. Tan, X. W. Sun, Z. G. Yu, P. Wu, G. Q. Lo and D. L. Kwong, Applied Physics Letters **91** (7), 072101 (2007).

10. X. Li, S. E. Asher, S. Limpijumnong, S. B. Zhang, S.-H. Wei, T. M. Barnes, T. J. Coutts and R. Noufi, Journal of Vacuum Science & Technology A **24** (4), 1213-1217 (2006).

11. H. S. Hsu, Y. Tung, Y. J. Chen, M. G. Chen, J. S. Lee and S. J. Sun, physica status solidi (RRL) – Rapid Research Letters **5** (12), 447-449 (2011).

12. D. K. Mishra, J. Mohapatra, M. K. Sharma, R. Chattarjee, S. K. Singh, S. Varma, S. N. Behera, S. K. Nayak and P. Entel, Journal of Magnetism and Magnetic Materials **329**, 146-152 (2013).

13. S. Sakong and P. Kratzer, Semiconductor Science and Technology **26** (1) (2011).

14. A. El Amiri, H. Lassri, E. K. Hlil and M. Abid, Journal of Magnetism and Magnetic Materials **374**, 338-341 (2015).

15. R. Khalid, K. Yaqub, S. Yaseen, S. Javeed, A. Ashraf, S. A. Janjua and S. Ahmad, Nuclear Instruments and Methods in Physics Research Section B: Beam Interactions with Materials and Atoms **263** (2), 497-502 (2007).

16. S. Chakrabarti, D. Ganguli and S. Chaudhuri, Materials Letters **58** (30), 3952-3957 (2004).

17. Z. G. Wang, X. T. Zu, S. Z. Yang and L. M. Wang, Journal of Materials Science **41** (12), 3729-3733 (2006).

18. A. Younis, D. Chu and S. Li, Nanoscale Research Letters **8** (1), 1-6 (2013).

19. H. Hosono, in *Handbook of Advanced Ceramics (Second Edition)* (Academic Press, Oxford, 2013), pp. 455-487.

20. S. Zhou, Q. Xu, K. Potzger, G. Talut, R. Grötzschel, J. Fassbender, M. Vinnichenko, J. Grenzer, M. Helm, H. Hochmuth, M. Lorenz, M. Grundmann and H. Schmidt, Applied Physics Letters **93** (23), 232507 (2008).

21. R. D. Shannon, Acta Crystallographica Section A **32** (5), 751-767 (1976).

22. O. Haibo, H. J. Feng, L. Cuiyan, C. Liyun and F. Jie, Materials Letters **111**, 217-220 (2013).

23. C. S. Wei, S. P. Lau, M. Tanemura, M. Subramanian and Y. Akaike, Applied Surface Science **258** (14), 5486-5489 (2012).

24. S. B. Zhang, S. H. Wei and A. Zunger, Physical Review B **63** (7), 075205 (2001).

25. J. Moulder, W. Stickle, P. Sobol and K. Bomben, *Handbook of X-Ray Photoemission Spectroscopy*: *a reference book of standard spectra for identification and interpretation of XPS data.* Perkin-Elmer Corp., Physical Electronics Division, Eden Prairie, Minnesota, USA (1995).

26. L. Kameswara Rao and V. Vinni, Applied Physics Letters **63** (5), 608-610 (1993).

27. G. Tyuliev and S. Angelov, Applied Surface Science **32** (4), 381-391 (1988).

28. F. Li, C. Zhang, P. Wang and P. Li, Physica E: Low-dimensional Systems and Nanostructures **47**, 34-39 (2013).

29. R. H. Kodama, Journal of Magnetism and Magnetic Materials **200** (1–3), 359-372 (1999).

30. P. V. Hendriksen, S. Linderoth and P. A. Lindgård, Physical Review B **48** (10), 7259-7273 (1993).

31. A. Saif Ullah, S. K. Hasanain, F. B. Massimo and G. H. Jaffari, Journal of Physics: Condensed Matter **25** (15), 156005 (2013).

32. D. Kim, J.-h. Yang and J. Hong, Journal of Applied Physics **106** (1), 013908 (2009).

33. K. Parmod, K. M. Hitendra and K. Asokan, EPL (Europhysics Letters) **110** (6), 67006 (2015).

34. X.-L. Li, G. Jun-Feng, Z.-Y. Quan, X.-H. Xu and G. A. Gehring, IEEE Transactions on Magnetics **46** (6), 1382-1384 (2010).

35. T. S. Herng, S. P. Lau, C. S. Wei, L. Wang, B. C. Zhao, M. Tanemura and Y. Akaike, Applied Physics Letters **95** (13), 133103 (2009).

36. J. W. Park, D. H. Kim, S.-H. Choi and M. L. a. D. Lim, Journal of the Korean Physical Society **Vol. 57** (6), 1482-1485 (2010).